Asian Journal of Pharmaceutical Sciences 14 (2019) 521–530

Available online at www.sciencedirect.com

ScienceDirect

journal homepage: www.elsevier.com/locate/AJPS

Original Research Paper

# Exploring the relationship of hyaluronic acid molecular weight and active targeting efficiency for designing hyaluronic acid-modified nanoparticles

*Lu Zhong*[a], *Yanying Liu*[a], *Lu Xu*[a], *Qingsong Li*[a], *Dongyang Zhao*[a], *Zhenbao Li*[a], *Huicong Zhang*[a], *Haotian Zhang*[b], *Qiming Kan*[b], *Jin Sun*[a,*], *Zhonggui He*[a,*]

[a] *Wuya College of Innovation, Shenyang Pharmaceutical University, Shenyang 110016, China*
[b] *School of Pharmacy, Shenyang Pharmaceutical University, Shenyang 110016, China*

ARTICLE INFO

*Article history:*
Received 30 July 2018
Revised 12 October 2018
Accepted 4 November 2018
Available online 6 December 2018

*Keywords:*
Hyaluronic acid
Molecular weight
Active targeting efficiency
CD44 receptor
Potential mechanism

ABSTRACT

Although it is reported that the targeting ability of hyaluronic acid (HA)-based nanoparticles (NPs) is molecular weight (MW) dependent, the influence of HA MW on targeting efficiency of HA-functionalized NPs and the underlying mechanism remain elusive. In this study, we constituted three HA-functionalized Dox-loaded NPs (Dox/HCVs) different HA MWs (7, 63, and 102 kDa) and attempted to illustrate the effects of HA MW on the targeting efficiency. The three Dox/HCVs had similar physiochemical and pharmaceutical characteristics, but showed different affinity to CD44 receptor. Furthermore, Dox/HCV-63 exerted the best targeting effect and the highest cytotoxicity compared with Dox/HCV-7 and Dox/HCV-102. It was interesting to found that both the HA-CD44 binding affinity and induced CD44 clustering by HA-based NPs were HA MW-dependent, the two of which determine the apparent targeting efficacy of Dox/HCV NPs in the conflicting directions. Those results laid a good foundation for rationally designing HA-based NPs in cancer therapy.



## 1. Introduction

Comparing with conventional nontargeted nanoparticulate drug delivery systems (Nano-DDS), active targeting Nano-DDS has attracted great attention due to enhanced therapeutic effect and reduced undesirable side effects. They are usually fabricated by modifying nanocarriers with active targeting moieties which recognize specific biomarkers on the surface of tumor cells, such as antibody [1], nucleic acid [2], peptide [3], hyaluronic acid [4], some essential nutrients related

* Corresponding authors. Wuya College of Innovation, Shenyang Pharmaceutical University, Shenyang 110016, China. Tel.: +86 24 23986321
*E-mail addresses:* sunjin@syphu.edu.cn (J. Sun), hezhgui_student@aliyun.com (Z. He).
Peer review under responsibility of Shenyang Pharmaceutical University.

https://doi.org/10.1016/j.ajps.2018.11.002

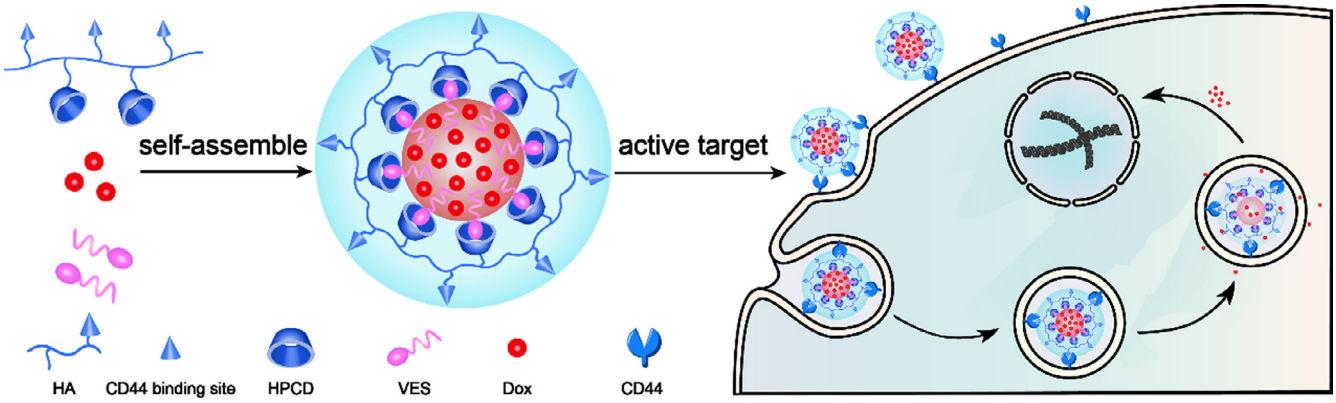


**Scheme 1 – Schematic of self-assembled Dox/HCVs nanoparticles and illustration of internalization procedure of nanoparticles. Active targeting Dox-loaded nanoplatform (Dox/HCVs) was self-assembled by HPCD grafted HA conjugates (HA-CD) with the help of the inclusion interaction of cyclodextrin and the bridging effect of VES. The core–shell nanoparticles will be internalized via HA-CD44 interaction by tumor cells to achieve the targeting delivery.**

transporters like biotin [5], amino acid [6], folate [7] and other various ligands. Among them, hyaluronic acid (HA) draws a great of attention due to its good properties.

HA is a natural occurrence linear anionic glycosaminoglycan polymer with a wide range of sizes composed of a simple repeating disaccharide of D-glucuronic acid and N-acetyl-D-glucosamine linked with a glucuronidic $\beta$ (1,3) bond and is ubiquitous in tissues and fluids. HA possesses superior characteristics in water solubility, biocompatibility, biodegradation, non-toxicity, and non-immunogenicity [8,9]. Together with the abundance of readily-modified carboxyl and hydroxyl groups, it has been widely utilized as carrier to deliver low-molecule weight drug [10–12], antibody [13], nucleic acid [14], protein [15] and tissue engineering [16,17], etc. HA abundantly exists in extracellular matrix to exhibit vital multiple physiological functions by interacting with its specific receptors called hyaladherins, including CD44, lymphatic vessel endothelial HA receptor (LYVE-1), inter-$\alpha$-inhibitor (I$\alpha$I), CD38, receptor for HA-mediated motility (RHAMM, also called CD168) and tumor necrosis factor-stimulated gene-6 (TSG-6) [18–20], etc. Therein CD44 is a principal hyaladherins and a trans-membrane glycoprotein participating in diverse significant cellular functions, such as cell proliferation, differentiation, migration, angiogenesis and mediates cellular endocytosis of HA for degradation [8,20–22]. In addition, CD44 is usually overexpressed in many kinds of malignant tumor cells, and many studies have demonstrated that nanoparticles modified with HA exerted better tumor targeting effect due to HA-CD44 specific interaction [23–27].

It has been found that HA molecular weight (MW) determines its diverse physiological functions, including cell migration, proliferation, angiogenesis, and gene expression and so on [28,29]. As for HA-based active targeting Nano-DDS, HA MW also affects its active targeting efficiency. For instance, $Fe_3O_4$ NPs coated with 31 kDa HA showed a better targeting ability to Hela cells than 6 kDa HA [30] and the cellular uptake of HA-grafted liposomes was improved with increase of HA MW (5–8 < 10–12 < 175–350 kDa) [31]. Similar conclusions also have been achieved by other reports [32–34]. On the contrary, there are some different findings, for example, the photodynamic therapy HACE NPs based on 20 kDa HA exerted better intracellular uptake capability and therapeutic efficacy than those based on 50 kDa and 100 kDa HA [35].

In this work, we intended to explore the relationship of HA MW and active targeting efficiency for HA-functionalized Nano-DDS and then to provide reliable scientific valid guidance for designing HA-based NPs. Based on our previous studies [36], we modified HA covalently with hydroxypropyl-$\beta$-cyclodextrin (HPCD) to prepare three different MWs HA-based nanocarriers, and then assembled Doxorubicin (Dox)-loaded nanoparticles (labeled as Dox/HCVs) by the host-guest inclusion interaction of cyclodextrin and bridging effect of vitamin E succinate (VES) (Scheme 1). We further investigated their physiochemical and pharmaceutical properties, evaluated cellular active targeting efficacy and probed the underlying mechanism.

## 2. Materials and methods

### 2.1. Materials

Sodium hyaluronate (HA, MW = 7, 63, 102 kDa) was obtained from Frida biological engineering Co. Ltd. (Shandong, China). Hydroxypropyl-$\beta$-cyclodextrin (HPCD) was kindly supplied by Shijiazhuang Pharmaceutical Group Co. Ltd. (Hebei, China). mPEG5000 and vitamin E succinate (VES) were purchased from Sigma-Aldrich (St, Louis, MO, USA). 1-Ethyl-3-(3-dimethyalminopropl) carbodiimide (EDC) was purchased from Shanghai Haiqu Pharm Co. Ltd and 1-hydroxybenzotriazole (HOBT) was obtained from Pukang Pharm Co. Ltd. (Zhejiang, China). Cell culture medium Dulbecco's modified eagle's medium (DMEM) and Roswell Park Memorial Institute-1640 (RPMI-1640) were purchased from Gibco, Invitrogen Corp. (Carlsbad, California, USA). Fetal bovine serum (FBS), 3-(4,5-dimthy-2 -thiazolyl)-2,5-dipphenyl-2H-terazolium bromide (MTT), 4-(2-hydroxyethyl)-1-piperazinee -thanesulfonic

acid (HEPES), trypsin and other materials for cell culture were provided by Dalian Meilun Biotechnology Co. Ltd. Doxorubicin hydrochloride (Dox•HCl) was purchased from Huafeng United Technology Co. Ltd. (Beijing, China), and it was deprotonated with twice molar amount of triethylamine before use. Other organic solvents or reagents used were analytic grade.

### 2.2. Synthesis and characterization of HPCD grafted HA conjugates (HA-CDs)

To synthesize HPCD grafted HA conjugates, HA (0.2 g, 0.5 mmol), EDC (0.2 g, 1 mmol) and HOBT (0.11 g, 1 mmol) were dissolved in 5 ml anhydrous formamide and stirred in ice-bath for 2 h. Then, 0.5 g HPCD dissolved in anhydrous formamide was dropwise into the reaction solution with stirring. After the reaction solution was stirred at 40 °C for 48 h with the protection of $N_2$, the mixture was dialyzed against distilled water for a week (four times changes one day and the MW cut off 3500 Da) and then lyophilized after filtration to gain white powder HA-CDs. The structures of conjugates were confirmed by $^1$H nuclear magnetic resonance spectrometer ($^1$H NMR, Bruker-600 MHz, Switzerland) and fourier infrared spectrometer spectroscopy (FT-IR, IFS55, Bruker, Switzerland). For FT-IR, the samples were pressed with KBr and scanned from 4000 to 400 $cm^{-1}$ under vacuum. The HPCD grafting density (degree of substitution, DS) was calculated by the peak areas of the characteristic peak of HA around 2 ppm ($A_{2ppm}$) and HPCD around 5 ppm ($A_{5ppm}$) according to the following formula:

$$DS\ (\%) = (A_{5ppm}/A_{2ppm}) \times (3/7) \times 100\%$$

where 7 is the number of hydrogen atom in HPCD (H (1,1′)) and 3 is the number of hydrogen atom of $–CH_3$ in HA [37].

$^1$H NMR (600 MHz, D2O, TMS, $\delta$): 1.01(s, –CH3- of hydroxypropyl); 1.88 (s, –CH3- of HA); 4.43 (S, H (1,1′) of HA glycoside); 4.94 (d, H (1,1′) of HPCD glycoside); 3.07–3.89 (m, H signals of HA glycoside)

### 2.3. Preparation and characterization of Dox-loaded HA-CDs nanoparticles (Dox/HCVs)

Nanoparticles were prepared by emulsion solvent evaporation method. Briefly, 2 mg VES was dissolved in 1 ml dichloromethane (DCM) then the solution was poured into 4 ml HEPES buffer (pH 7.4) which contains 10 mg HA-CD, then the mixture was under sonication for 10 min at 100 W (turn on for 2 s with a 3 s interval) in ice bath by a probe-type sonifier. Afterward, it was evaporated to remove the DCM under reduced pressure with a rotary evaporator and centrifuged 10 min at 13000 rpm, and then filtered through 0.45 μm filter to gain the final preparations. For getting the Dox-loaded nanoparticles, the same procedure was carried out except for dissolving another 0.5 mg Dox in DCM.

The size, zeta potential and polydispersion index (PDI) were detected by dynamic light scattering (DLS) using Malvern Zetasizer instrument (Nano ZS, Malvern, UK) at 25 °C. The colloidal stability of preparations was explored by determining the particle size at time intervals by DLS. The micelle morphology was observed by JEM-2100 trans-mission electron microscope (TEM, JEOL, Japan). Negatively stained method was used on a carbon-coated copper grid with 2% phosphotungstic acid. The encapsulation efficiency (EE) and drug-loading content (DL) were measured by a UV–vis spectrometer at 485 nm. In general, the prepared nanoparticles (uncentrifuged) and the centrifugal supernatant were diluted with methanol and treated with ultrasonic to destroy the structure of nanoparticles and dissolve the Dox completely, then the Dox contents were measured. Meanwhile, a certain amount of drug ($M_{Dox}$) was measured precisely, and the quality of total sample ($M_{Total}$) was weighted after lyophilization. The EE and DL were calculated using following formulas.

$$EE\ (\%) = Dox_{suspernatant}/Dox_{uncentrifuged} \times 100\%$$
$$DL\ (\%) = M_{Dox}/M_{Total} \times 100\%$$

### 2.4. In vitro release profiles of Dox-loaded preparations

The kinetics of drug efflux were studied as previously described [36]. Briefly, 1 ml preparation was packaged in dialysis membrane bag (MW cut-off 14 kDa), then was immersed in 30 ml PBS (pH 7.4, pH 6.5 and pH 5) with a continuously shaking at 100 rpm at 37 °C. At designated periods, 1 ml of medium was extracted and another 1 ml fresh medium was refilled. The concentrations of Dox were measured by HPLC method after filtrating by 0.22 μm filter membrane.

### 2.5. Cell culture growth and maintenance

Monolayers of cells were grown with 10 cm dishes in an incubator at 37 °C with 5% $CO_2$ and 95% relative humidity. Hela cells and MCF-7 cells were cultured in Dulbecco's modified Eagle's medium (DMEM) containing 10% FBS and 1% penicillin-streptomycin. H460 cells and A549 cells were maintained in RPMI 1640 medium containing 10% FBS and 1% penicillin-streptomycin. The cells were subculture with 0.25% trypsin-EDTA in PBS.

### 2.6. Analysis of cell surface CD44

For flow cytometry, the presence of CD44 on the cell surface was detected by indirect staining with secondary antibody (Dlight-488 conjugated IgG) [25,32,38]. Firstly, cells were plated on glass cover slips in 6-well plate for 24 h, washed twice with PBS buffer and treated with 0.25% trypsin-EDTA to collect cells. Then cells were fixed with 4% paraformaldehyde (PFA), permeabilized by 0.1% Triton-X 100, incubated with anti-CD44 antibody (Abcam119348, 1:200) overnight at 4 °C, the negative control sample were incubated with isotype antibody (Affymetrix eBioscience, 14-4031). Then samples were treated with Dlight-488 conjugated secondary antibody for 30 min at room temperature. After washing with PBS three times, the samples were resuspended in PBS and analyzed by flow cytometry (BD Biosciences, Oxford, UK).

For immunofluorescence method, $1 \times 10^5$ cells/well cells were seeded on glass cover slips in 24-well plate to grow overnight. After washed twice with PBS and fixed with 4% paraformaldehyde (PFA), the cells were incubated overnight with the primary antibody (Abcam119348, 1:200) at 4 °C and then for 30 min with the secondary antibody at room temperature. The nuclei were stained with DAPI for 10 min. Finally,

**Table 1 – Physiochemical and pharmaceutical characteristics of Dox/HCVs. All data was shown as mean ± standard deviation (mean ± SD, $n = 3$).**

| Dox/HCVs | Size (nm) | PDI | Zeta (mv) | EE (%) | LD (%) |
|---|---|---|---|---|---|
| Dox/HCV-7 | 137. 2 ± 1.65 | 0.17 ± 0.0004 | −31.5 ± 0.153 | 93.25 ± 2.007 | 2.66 ± 0.3867 |
| Dox/HCV-63 | 141.1 ± 1.528 | 0.181 ± 0.014 | −33.9 ± 0.643 | 91.42 ± 3.8215 | 2.57 ± 0.28 |
| Dox/HCV-102 | 140.7 ± 0.889 | 0.181 ± 0.058 | −33.2 ± 0.321 | 93.12 ± 1.6618 | 2.35 ± 0.1099 |

the slides were mounted with antifade mounting medium (Beyotime, P0126) and samples were visualized using confocal laser scanning microscopy (CLSM, Nikon C2SI, Japan).

To visualize the CD44 receptors change of existence forms and distribution, we pretreated cells with non-drug-loaded nanoparticles (HCVs) for presupposed time and then disposed them according to the above process.

### 2.7. *Proliferation inhibition experiments*

The proliferation inhibition of various formulations was evaluated using classical MTT method. Cells were plated in 96-well cell culture plates (5000 cells/well) and incubated overnight at 37 °C. Cells were treated with varies of concentrations of Dox, Dox/HCV-7, Dox/HCV-63, Dox/HCV-102 for 48 h. After aspirating the treatment medium, 100 µl of fresh medium and 20 ul of MTT solution (5 mg/ml) were added to the cells. After 4 h incubation, plates were read at 570 nm using a BioRad microplate reader (Model 500, USA). The cells treated with medium without drugs were treated as negative controls. The log dose-response curve was plotted and the median inhibitory concentration ($IC_{50}$) was calculated with the software GraphPad Prism 5.

### 2.8. *Cellular uptake of Dox/HCVs*

Briefly, the cells were plated on a 6-well plate (0.5 million cells per well) and cultured for 24 h, and the various preparations diluted with serum-free media (the final concentration of 10 µg/ml of Dox) were added to the cells, with serum-free medium-treated cells as control. After 1 h or 3 h of incubation at 37 °C, the medium was discarded and the cells were washed three times with ice-cold PBS, harvested by centrifugation (3000 rpm, 5 min), washed with PBS three times again. At last, the cells were resuspended in 0.3 ml PBS for analysis based on the fluorescence of Dox by flow cytometer.

### 2.9. *Potential mechanism of nanoparticle endocytosis*

The potential endocytic mechanisms of nanoparticles were performed with the method reported before [39]. Hela cells were seeded in 6-well plate (0.5 million cells per well) and cultured for 24 h. Chlorpromazine hydrochloride (CPZ, 10 µg/ml), colchicine (8 µg/ml), quercetin (6 µg/ml), indomethacin (6 µg/ml) and free HA (MW 102 kDa, 5 mg/ml) were added to each well and pre-incubated for 1 h, respectively. Then the mediums were replaced with Dox/HCVs nanoparticles (the final concentration of 10 µg/ml of Dox) along with the corresponding endocytic inhibitors (the same concentration as pre-incubation) and the cells treated only with nanoparticles were as control. After culturing for 3 h at 37 °C, the cells were washed with cold PBS, harvested and analyzed using flow cytometer. In addition, we investigated the effect of energy on endocytosis by measuring the corresponding uptakes of Dox/HCVs at 4 °C.

## 3. Results and discussion

### 3.1. *The synthesis and characterization of HA-CDs*

HA with too large MW has some limitations for Nano-DDS, such as large particle size, wide size distribution and high viscosity [31,35,40]. Therefore, we chose series HA with MW 7, 63 and 102 kDa to modify in the study. HA was successfully functionalized by HPCD with the aid of catalysts EDC and HOBT. The synthesis procedure of HA-CD was illustrated in Fig. S1 and the chemical structure was confirmed by $^1$H NMR, as shown in Fig. S2. Based on the $^1$H NMR spectra, the average degree of substitution was calculated to be about 50% HPCD grafting (Table S1) for three kinds of conjugates. In Fig. S3, by comparing the FT-IR spectra of HA, HPCD and HA-CD, a new specific band at 1755 $cm^{-1}$ was observed in HA-CD due to the stretching vibration absorption of the formed ester linkage, confirming the successful synthesis of HA-CDs with three different HA MWs.

### 3.2. *Characterization of Dox/HCVs*

Dox/HCVs were prepared with a slight modification based on our previous study [36]. The long alkyl chains of VES could be inserted into the CD cavity with host-guest inclusion interaction, and the other hydrophobic segments of VES would constitute a hydrophobic core capable of loading Dox. The hydrophilic hyaluronan would surround the hydrophobic core, finally resulting in a core-shell nanostructure. The physiochemical and pharmaceutical characteristics of Dox/HCVs with three different HA MWs were summarized in Table 1. All nanoparticles showed a uniform size distribution and spherical shape morphology (Fig. 1A, B and Fig. S4), and possessed similar particle size (~140 nm) and zeta potential (~−30 mv). And the EE of three NPs were more than 90%. The similar characteristics of Dox/HCVs should be attributed to the tight hydrophobic core interaction. The change of average diameters of Dox/HCVs was observed for ten days stored at 4 °C. As shown in Fig. 1C, all Dox/HCVs had barely change in particle size, suggesting that the obtained preparations exhibited excellent colloidal stability. It might benefit from the good hydrophilic and surface negative charge of HA. The release

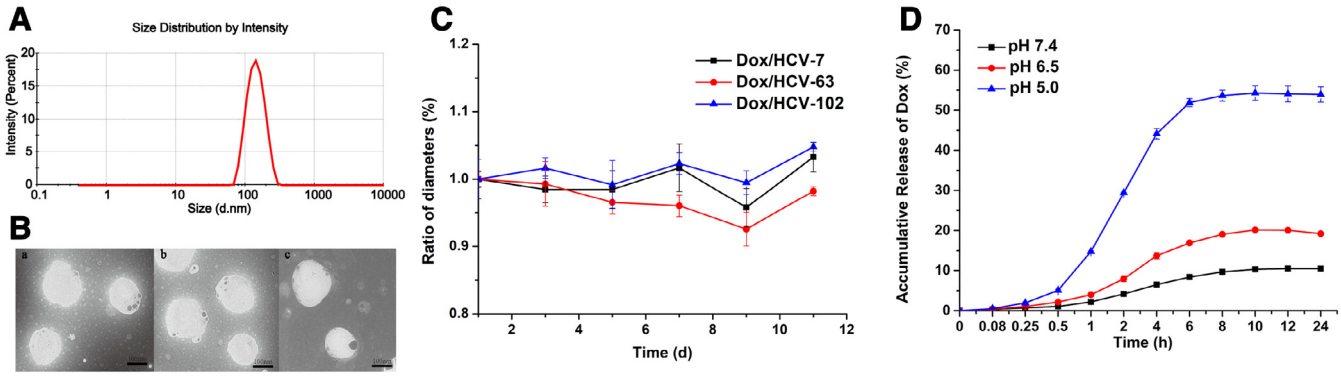


**Fig. 1 – Physiochemical and pharmaceutical characteristics of Dox/HCVs: (A) size distribution by intensity of Dox/HCV-7; (B) morphology observation of Dox/HCV-7 (a), Dox/HCV-63 (b), Dox/HCV-102 (c) by TEM (the scale bar was 100 nm); (C) Colloidal stability of Dox/HCVs stored at 4 °C; (D) *In vitro* drug release behaviors of Dox/HCV-7 in PBS (pH 7.4, pH 6.5 and pH 5).**

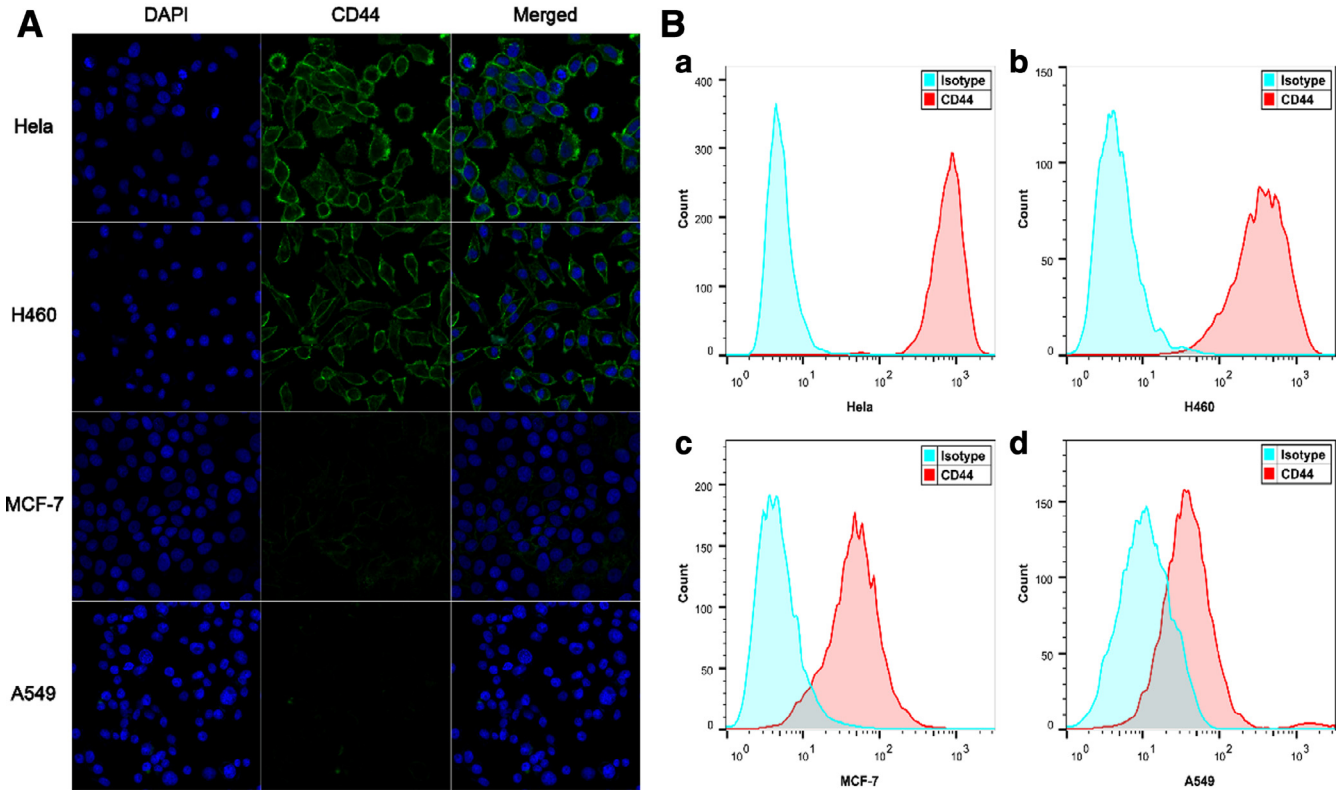


**Fig. 2 – (A) Analysis of surface CD44 receptor by immunofluorescence image with CLSM on various tumor cells; (B) CD44 receptor expression was measured on Hela (a), H460 (b), MCF-7 (c) and A549 (d) cells by flow cytometry.**

behavior of Dox at 37 °C for 24 h under different pH conditions was carried out. As shown in Fig. 1D, the accumulative release of Dox from Dox/HCV-7 NPs in 6 h was only 8.37% at pH 7.4, 16.9% at pH 6.5, but 51.91% at pH 5, suggesting Dox release was pH-dependent which probably due to the protonation of doxorubicin at acidic environment [41,42]. The similar pattern was found in Dox/HCV-63 and Dox/HCV-102, as shown in Fig. S5. The distinct release property would be in favorable for targeted drug delivery, since it could avoid the Dox leakage during blood circulation (physiology condition pH value~7.4) while rapidly release drug once internalized by tumor cells (endosome and lysosome pH value 6.5–5 or even more lower).

HA as an active targeting ligand for CD44 receptor has attracted great attention in Nano-DDS and many reports demonstrated the active targeting efficiency of Nano-DDS was MW-dependent. But some investigation results were only based on free HA rather than HA-modified NPs. In addition, the physicochemical characteristics of NPs such as particle size, shape, surface chemical composition and so on, have a significant influence on their cellular internalization and intracellular delivery [43,44], but it was rarely taken into

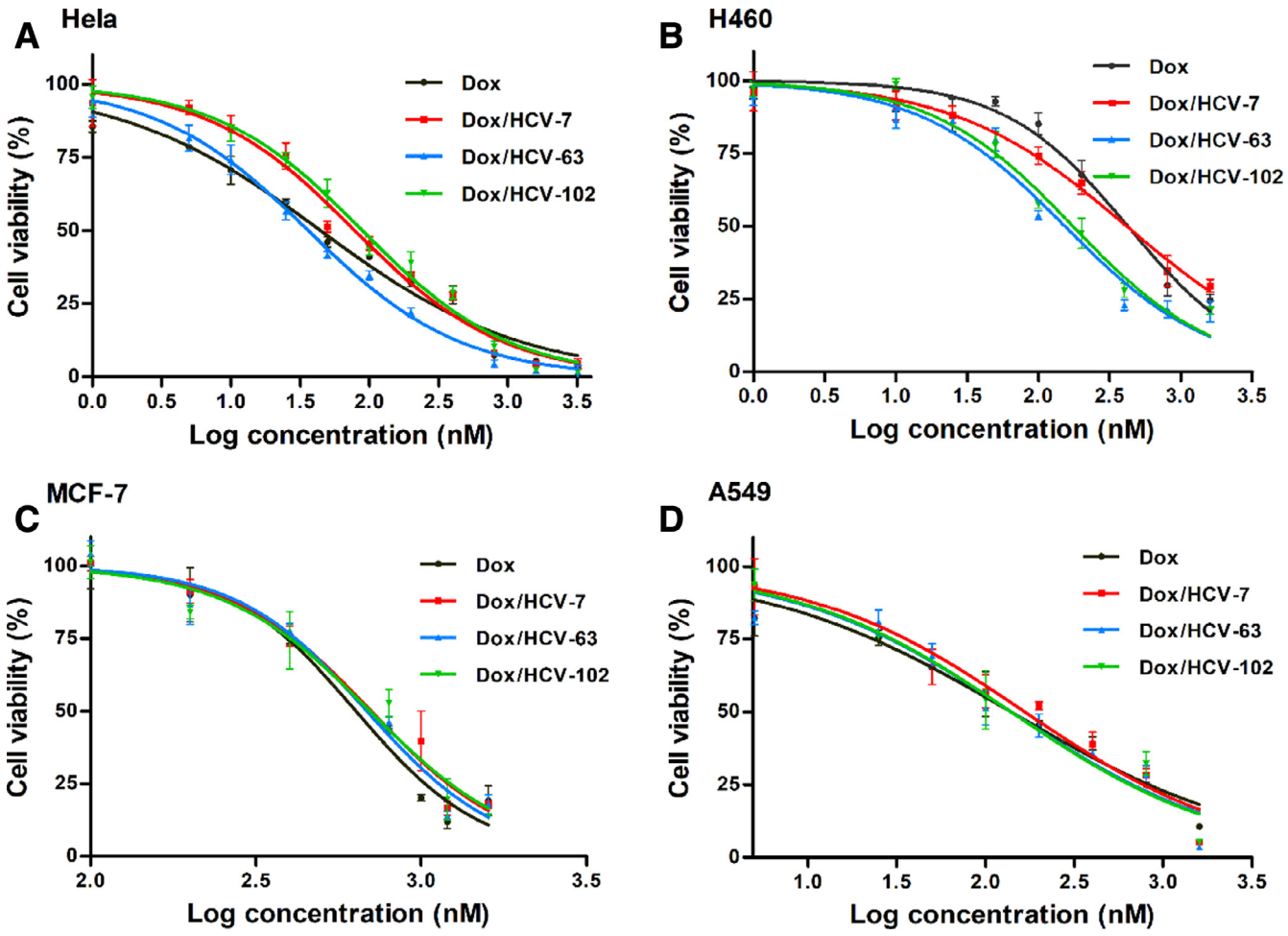


**Fig. 3 – Cell viabilities when treated with various formulations at different concentrations for 48 h on Hela (A), H460 (B), MCF-7 (C) and A549 (D) cells.**

consideration in many studies. The three HA-based NPs we prepared had the similar physicochemical and pharmaceutical characteristics, it laid a significant fundamental for illuminating the relationship between HA MW and its active-targeting efficacy.

### 3.3. *CD44 receptor expression analysis*

CD44 is a transmembrane glycoprotein overexpressed on the surface of a variety of cancer cells and is the most primary receptor of HA. It has been reported that CD44 density has a great effect on targeting efficiency [31]. With the aim to identify the suitable cell models for the further studies, the expression levels of CD44 on several cancer cells were conducted by confocal laser scanning microscope (CLSM). In Fig. 2A, the strong fluorescence intensity could be observed on the cell membranes of Hela and H460 cells, indicating CD44 overexpression. By contrast, there was little fluorescence signal on MCF-7 and A549 cells, indicating CD44 low-expression. CD44 expression levels were also evaluated with flow cytometric method, as shown in Fig. 2B. The mean fluorescence intensity (MFI) suggested that both Hela and H460 cells overexpressed CD44, but MCF-7 and A549 cells had a very low expression of CD44, which in consistent well with CLSM results. Next, Hela and H460 as positive cell models (CD44+), in contrast, MCF-7 and A549 as negative cell models (CD44-) were used for the following studies.

**Table 2 – $IC_{50}$ values (nM) of Dox, Dox/HCVs on different tumor cells for 48 h incubation.**

| Dox/HCVs | Hela | H460 | A549 | MCF-7 |
|---|---|---|---|---|
| Dox | 44.4 | 422.7 | 138.6 | 636.1 |
| Dox/HCV-7 | 78.7 | 415.4 | 165.5 | 707.5 |
| Dox/HCV-63 | 36.2 | 153.3 | 139.0 | 686.5 |
| Dox/HCV-102 | 89.2 | 174.4 | 138.5 | 701.6 |

### 3.4. *Influence of HA MW on cytotoxicity of Dox-loaded formulations*

Fig. 3 illustrated the cytotoxicity of free Dox and various Dox/HCVs at different concentrations on four cancer cells for

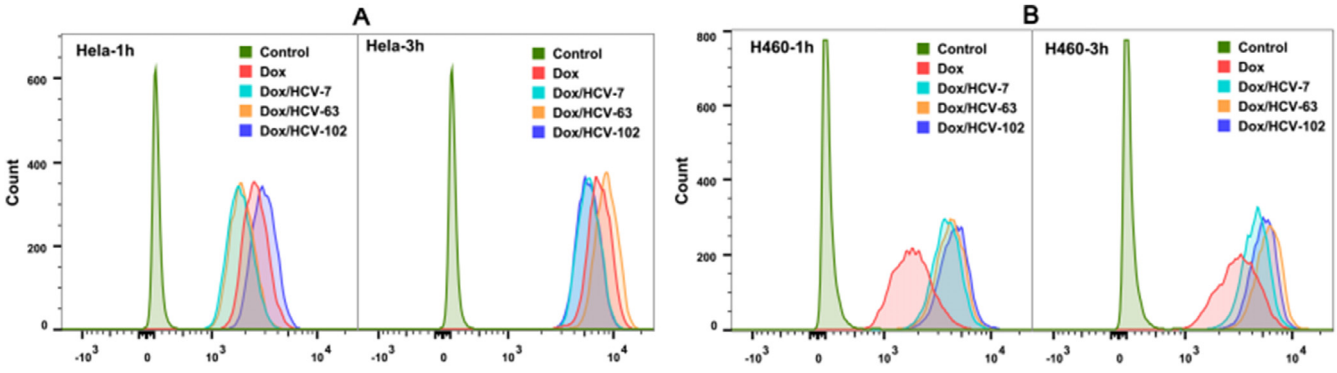


**Fig. 4 – Cellular uptakes of free Dox and Dox/HCVs on CD44 + cells Hela (A) and H460 (B) at 37 °C for 1 h and 3 h were measured by flow cytometry.**

48 h and Table 2 summarized the corresponding $IC_{50}$ values. There existed a big difference for $IC_{50}$ values of free Dox on four cancer cells, suggesting cytotoxicity being the cell type-dependent. In addition, among the three Dox-loaded NPs, there were different degrees of cytotoxic effects on Hela and H460 cells, but similar cytotoxicity on MCF-7 and A549 cells. It indicated that the targeting effect of Dox/HCVs was in a CD44-mediated manner and the HA MW may affect cytotoxic effect through adjusting cellular internalization capacity of NPs [38]. This result also agreed well with the previous results of CD44 expression. Furthermore, in comparison with Dox/HCV-7 and Dox/HCV-102, Dox/HCV-63 exhibited remarkably higher cytotoxicity on Hela cells (Fig. 3). It had the lowest $IC_{50}$ values (36.2 nM), much lower than Dox/HCV-7 (78.7 nM) and Dox/HCV-102 (89.2 nM). Additionally, the similar trend could be found on H460 cells.

### 3.5. *Effect of HA MW on cellular uptake of Dox/HCVs*

We further measured the cellular uptakes of nanoparticles on CD44 + and CD44- cells at 37 °C for 1 h and 3 h by flow cytometry. As shown in Fig. 4, S6 and S7, all formulations exerted a stronger MFI at 3 h than those at 1 h, indicating a time-dependent cellular uptake. And Dox/HCVs nanoparticles presented different MFI values on CD44 + cells, in sharp contrast to those on CD44- cells, confirming that CD44 receptor played a vital role in HA-mediated active targeting. On CD44 + Hela and H460 cells, Dox/HCV-63 showed the highest uptake of Dox at 3 h in comparison to Dox/HCV-7 and Dox/HCV-102, in well consistent with their cytotoxic effects. But it was interesting that Dox/HCV-102 exerted the better cellular uptake than others after incubation for 1 h at 37 °C.

### 3.6. *Potential mechanisms of nanoparticles endocytosis*

Due to the endocytic pathway also has a strong effect on the intracellular delivery of Nano-DDS [45], we investigated the potential mechanisms of Dox/HCVs endocytosis. As shown in Fig. 5A, a dramatic decrease of cellular uptakes could be observed at 4 °C for Dox/HCVs, suggesting the cellular endocytosis of NPs was energy-consuming. Furthermore, several endocytic inhibitors were chosen to investigate the specific mechanisms. Chlorpromazine is an inhibitor interrupting the clathrin-dependent endocytosis by dissociating clathrin and adapter proteins from the membrane [45], and colchicine can block the macropinocytosis through interfering the microtubule transportation [46], while indomethacin and quercetin are inhibitors for caveolae-mediated endocytosis and caveolae-/clathrin-independent endocytosis respectively [47]. In Fig. 5A, HA MW had a negligible influence on their endocytic pathways. And the cellular uptakes of Dox/HCVs treated with chlorpromazine were significantly decreased by about 50%, but no significant changes were observed for other inhibitors. Those results indicated that the cellular internalization of Dox/HCVs was primarily mediated by clathrin-mediated endocytosis.

Aim to understand the role of CD44 receptor during NPs internalization, a competitive uptake inhibition was carried out on Hela cells pre-added excessive free HA with the largest molecule weight (102 kDa) to saturate the CD44 receptor by multivalent interactions. In Fig. 5B, the cellular uptakes of the three Dox/HCV NPs were all significantly decreased, further confirming CD44-dependent endocytosis for HA-based Nano-DDS [10,48]. In addition, the decreasing percentages of Dox/HCV-7 (47.45%) and Dox/HCV-63 (50.97%) were slightly higher than Dox/HCV-102 (40.64%), owing to the highest binding affinity of 102 kDa HA with CD44 receptor [34].

### 3.7. *Influence of HA MW on the binding affinity of Dox/HCVs*

The binding affinity of Dox/HCVs to CD44 receptor was further estimated by measuring their cellular uptake at 4 °C for 3 h, which impedes the following endocytosis process after NPs binding to cell plasma membrane. As shown in Fig. 6 and Fig. S8, Dox/HCVs showed similar MFI as free Dox on CD44- cell lines, but higher MFI than free Dox on CD44 + cells, due to the specific HA-CD44 interaction. Comparing the MFI values of Dox/HCVs, their binding affinities followed an order of Dox/HCV-102>Dox/HCV-63>Dox/HCV-7, and the tendency was more apparent on Hela cells. This result agreed with the previous reports that higher MW HA exhibited greater affinity ability to CD44 via the multivalent binding interaction [30–

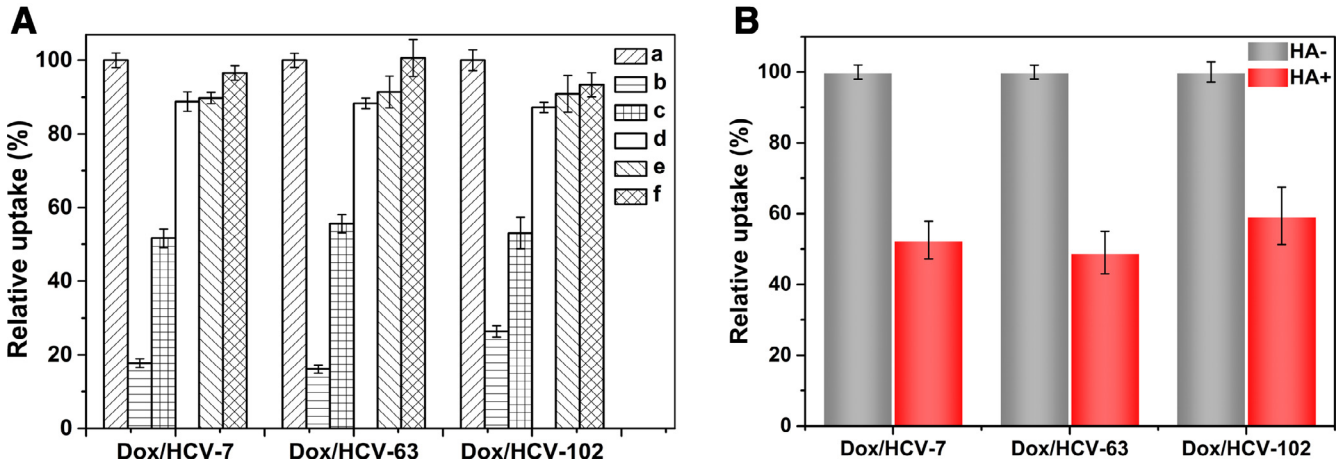


**Fig. 5 – (A) Effects of endocytosis inhibitors on cellular uptakes of Dox/HCVs were studied by flow cytometry: Hela cells were incubated with medium containing fixed Dox concentration formulations without (a, control; b, at 4 °C) or with 10 mg/ml chlorpromazine(c), 8 mg/ml colchicine(d), 6 mg/ml indomethacin(e) and 6 mg/ml quercetin (f) for 3 h after pretreated with inhibitors for 1 h at 37 °C. (B) Effect of competitive inhibition of free HA (MW 102 kDa, 5 mg/ml) on cellular uptake of Dox/HCVs at 37 °C for 3 h.**

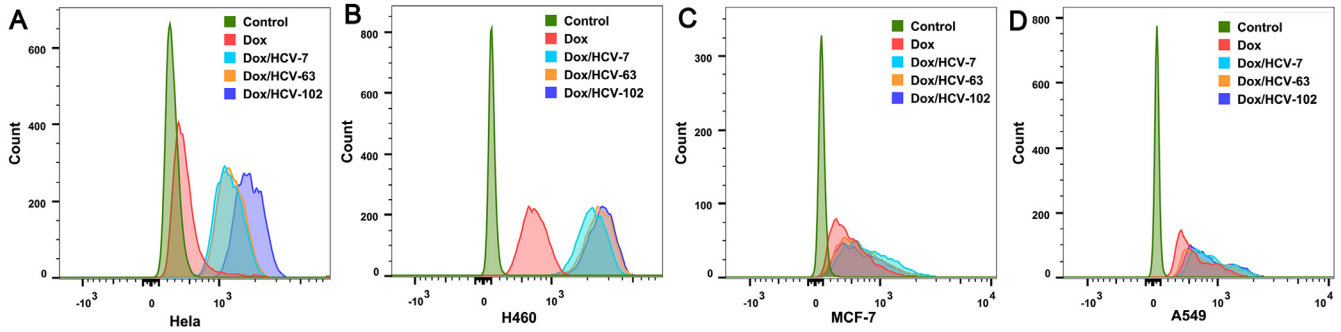


**Fig. 6 – Binding affinity of various Dox/HCVs was studied by investigated uptake at 4 °C for 3 h on Hela (A), H460 (B), MCF-7 (C) and A549 (D) cells by flow cytometry.**

33,49]. It might explain that Dox/HCV-102 exerted the better cellular uptake when incubation for 1 h at 37 °C (Fig. 4).

### 3.8. *Effect of Dox/HCVs towards to CD44 receptors*

Some studies reported that free large MW HA can trigger CD44 clustering but low MW HA or hyaluronidase can disrupt this process. And CD44 clustering not only involves in HA MW-dependent CD44-mediated cell signaling [20,50], but also participates in regulating the binding ability of HA to CD44 receptors [51–53]. In addition, receptor clustering has been observed in some active targeting NPs based on integrins and epidermal growth factor receptor, and was reported to decrease the apparent binding affinity of ligand to receptor [54]. Inspired by those findings, we observed the change of CD44 receptors on Hela cells after incubation with blank NPs HCVs for periods of time using CLSM (Fig. 7). In the control group, the fluorescence signals of CD44 receptors were uniformly distributed on the cell surface. By contrast, some granular fluorescence points appeared in HCVs groups and the

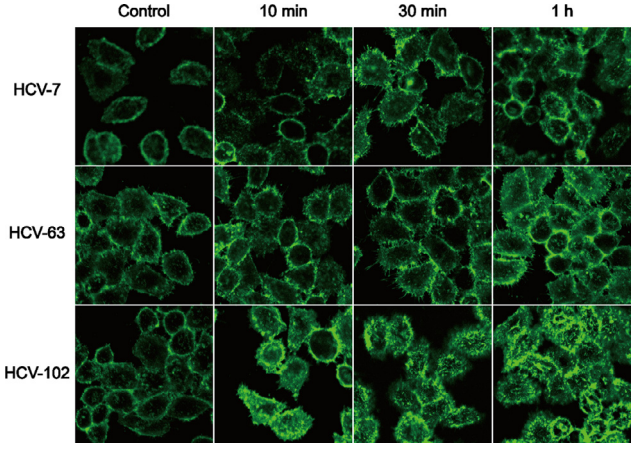


**Fig. 7 – The change of existence forms and distributions of CD44 receptors on Hela cells before and after incubation with blank nanoparticles HCVs for periods of time were observed by CLSM.**

distribution of receptors was uneven when incubated for only 10 minutes, representing the formation of CD44 clustering, especially in HCV-102 group. Furthermore, more fluorescence signals could be found within cells, probably as the result of the internalization of CD44 receptors along with NPs into cells. It is known that HA is internalized into cells via CD44-mediated endocytosis and then delivered to endosomes, finally transferred and degraded within the lysosomes [20,22,55]. With the increase in incubation time, increased CD44 clustering could be found, in particular for the HCV-102 group.

Above results indicated that HCV-102 induced more CD44 receptor clustering than HCV-7 and HCV-63. It might affect the overall targeting efficiency by decreasing the available number of CD44 receptors [56]. To a certain degree, it led to the lower cellular uptake at 3 h and cytotoxicity of Dox/HCV-102 when compared with Dox/HCV-63. Ultimately, binding affinity might be the rate-limiting step of cellular internalization at the early stage, but the apparent targeting efficacy was the combined result of binding affinity and induced CD44 clustering.

## 4. Conclusion

In this work, the three active targeting Nano-DDS with different MWs HA (7, 63, and 102 kDa) were prepared for exploring the effects of HA MW on the targeting efficiency. The three Dox/HCVs NPs had the similar physiochemical and pharmaceutical properties. Furthermore, the cell proliferation inhibition and cellular uptake experiments indicated that Dox/HCV-63 manifested better active targeting ability than Dox/HCV-7 and Dox/HCV-102. It was found that HA MW could tune the active targeting capacity of HA-based NPs via modulated binding affinity and induced CD44 clustering effect in a conflicting manner. The results might lay a reliable foundation and provide relative theoretical guidance for rationally designing HA-based Nano-DDS.

## Conflicts of interest

The authors report no conflicts of interest. The authors alone are responsible for the content and writing of this article.

## Acknowledgments

This work was supported by the National Basic Research Program of China (No. 81573371) and the key projects of Liaoning Province Department of Education (No. 2017LZD03).

## Supplementary material

Supplementary material associated with this article can be found, in the online version, at doi:10.1016/j.ajps.2018.11.002.

## REFERENCES

[1] Wang R, Li L, Zhang S, et al. A novel enediyne-integrated antibody-drug conjugate shows promising anti-tumor efficacy against CD30(+) lymphomas. Mol Oncol 2018;12(3):339–55.
[2] Xiang D, Shigdar S, Qiao G, et al. Nucleic acid aptamer-guided cancer therapeutics and diagnostics: the next generation of cancer medicine. Theranostics 2015;5:23–42.
[3] Sun Y, Gan W, Lei M, et al. PEPT1-mediated prodrug strategy for oral delivery of peramivir. Asian J Pharm Sci 2018;13(6):555–65.
[4] Stephen L, Hayward CLW, Kidambi S. Hyaluronic acid-conjugated liposome nanoparticles for targeted delivery to CD44 overexpressing glioblastoma cells. Oncotarget 2016;7(23):34158–71.
[5] Wang Z, Guo W, Kuang X, Hou S, Liu H. Nanopreparations for mitochondria targeting drug delivery system: current strategies and future prospective. Asian J Pharm Sci 2017;12:498–508.
[6] Bhutia YD, Babu E, Prasad PD, Ganapathy V. The amino acid transporter SLC6A14 in cancer and its potential use in chemotherapy. Asian J Pharm Sci 2014;9:293–303.
[7] Zhang P, He D, Klein PM, et al. Enhanced intracellular protein transduction by sequence defined tetra-oleoyl oligoaminoamides targeted for cancer therapy. Adv Funct Mater 2015;25:6627–36.
[8] Necas J, Bartosikova L, Brauner P, Kolar J. Hyaluronic acid (hyaluronan): a review. Vet Med 2008;53:397–411.
[9] Glucksam-Galnoy Y, Zor T, Margalit R. Hyaluronan-modified and regular multilamellar liposomes provide sub-cellular targeting to macrophages, without eliciting a pro-inflammatory response. J Control Release 2012;160:388–93.
[10] Zhong Y, Goltsche K, Cheng L, et al. Hyaluronic acid-shelled acid-activatable paclitaxel prodrug micelles effectively target and treat CD44-overexpressing human breast tumor xenografts *in vivo*. Biomaterials 2016;84:250–61.
[11] Noh I, Kim HO, Choi J, et al. Co-delivery of paclitaxel and gemcitabine via CD44-targeting nanocarriers as a prodrug with synergistic antitumor activity against human biliary cancer. Biomaterials 2015;53: 763–774.
[12] Martens TF, Remaut K, Deschout H, et al. Coating nanocarriers with hyaluronic acid facilitates intravitreal drug delivery for retinal gene therapy. J Control Release 2015;202:83–92.
[13] Wang C, Ye Y, Hochu GM, Sadeghifar H, Gu Z. Enhanced cancer immunotherapy by microneedle patch-assisted delivery of anti-PD1 antibody. Nano Lett 2016;16:2334–40.
[14] Yang X, Iyer AK, Singh A, et al. MDR1 siRNA loaded hyaluronic acid-based CD44 targeted nanoparticle systems circumvent paclitaxel resistance in ovarian cancer. Sci Rep 2015;5:8509.
[15] Fonte P, Araujo F, Silva C, et al. Polymer-based nanoparticles for oral insulin delivery: revisited approaches. Biotechnol Adv 2015;33:1342–54.
[16] Makris EA, Gomoll AH, Malizos KN, Hu JC, Athanasiou KA. Repair and tissue engineering techniques for articular cartilage. Nat Rev Rheumatol 2015;11:21–34.
[17] Takeda K, Sakai N, Shiba H, et al. Characteristics of high-molecular-weight hyaluronic acid as a brain-derived neurotrophic factor scaffold in periodontal tissue regeneration. Tissue Eng Part A 2011;17:955–67.
[18] Dosio F, Arpicco S, Stella B, Fattal E. Hyaluronic acid for anticancer drug and nucleic acid delivery. Adv Drug Deliver Rev 2016;97:204–36.

[19] Mattheolabakis G, Milane L, Singh A, Amiji MM. Hyaluronic acid targeting of CD44 for cancer therapy: from receptor biology to nanomedicine. J Drug Target 2015;23:605–18.
[20] Choi KY, Saravanakumar G, Park JH, Park K. Hyaluronic acid-based nanocarriers for intracellular targeting: interfacial interactions with proteins in cancer. Colloid Surf B 2012;99:82–94.
[21] D'Agostino A, Stellavato A, Corsuto L, et al. Is molecular size a discriminating factor in hyaluronan interaction with human cells? Carbohydr Polym 2017;157:21–30.
[22] Harada H, Takahashi M. CD44-dependent intracellular and extracellular catabolism of hyaluronic acid by hyaluronidase-1 and -2. J Biol Chem 2007;282:5597–607.
[23] Yen J, Ying H, Wang H, Yin L, Uckun F, Cheng J. CD44 Mediated nonviral gene delivery into human embryonic stem cells via hyaluronic-acid-coated nanoparticles. ACS Biomater – Sci Eng 2016;2:326–35.
[24] Sun D, Zhou JK, Zhao L, et al. Novel curcumin liposome modified with hyaluronan targeting CD44 plays an anti-leukemic role in acute myeloid leukemia *in vitro* and *in vivo*. ACS Appl Mater Inter 2017;9:16857–68.
[25] Lin CW, Lu KY, Wang SY, Sung HW, Mi FL. CD44-specific nanoparticles for redox-triggered reactive oxygen species production and doxorubicin release. Acta Biomater 2016;35:280–92.
[26] Shah KN, Ditto AJ, Crowder DC, et al. Receptor-mediated attachment and uptake of hyaluronan conjugates by breast cancer cells. Mol Pharm 2017;14:3968–77.
[27] Kim JE, Park YJ. High paclitaxel-loaded and tumor cell-targeting hyaluronan-coated nanoemulsions. Colloid Surf B 2017;150:362–72.
[28] Maharjan AS, Pilling D, Gomer RH. High and low molecular weight hyaluronic acid differentially regulate human fibrocyte differentiation. PLoS One 2011;6:e26078.
[29] Misra S, Hascall VC, Markwald RR, Ghatak S. Interactions between hyaluronan and its receptors (CD44, RHAMM) regulate the activities of inflammation and cancer. Front Immunol 2015;6:201.
[30] Li J, He Y, Sun W, et al. Hyaluronic acid-modified hydrothermally synthesized iron oxide nanoparticles for targeted tumor MR imaging. Biomaterials 2014;35:3666–77.
[31] Qhattal HS, Liu X. Characterization of CD44-mediated cancer cell uptake and intracellular distribution of hyaluronan-grafted liposomes. Mol Pharm 2011;8:1233–46.
[32] Arpicco S, Lerda C, Dalla Pozza E, et al. Hyaluronic acid-coated liposomes for active targeting of gemcitabine. Eur J Pharm Biopharm 2013;85:373–80.
[33] Mizrahy S, Goldsmith M, Leviatan-Ben-Arye S, et al. Tumor targeting profiling of hyaluronan-coated lipid based-nanoparticles. Nanoscale 2014;6:3742–52.
[34] Mizrahy S, Raz SR, Hasgaard M, et al. Hyaluronan-coated nanoparticles: the influence of the molecular weight on CD44-hyaluronan interactions and on the immune response. J Control Release 2011;156:231–8.
[35] Li W, Zheng C, Pan Z, et al. Smart hyaluronidase-actived theranostic micelles for dual-modal imaging guided photodynamic therapy. Biomaterials 2016;101:10–19.
[36] Han X, Li Z, Sun J, et al. Stealth CD44-targeted hyaluronic acid supramolecular nanoassemblies for doxorubicin delivery: probing the effect of uncovalent pegylation degree on cellular uptake and blood long circulation. J Control Release 2015;197:
29–40.
[37] Liu Y, Zhai Y, Han X, et al. Bioadhesive chitosan-coated cyclodextrin-based superamolecular nanomicelles to enhance the oral bioavailability of doxorubicin. J Nanopart Res 2014;16(10):2587.
[38] Lallana E, Rios de la Rosa JM, Tirella A, et al. Chitosan/hyaluronic acid nanoparticles: rational design revisited for RNA delivery. Mol Pharm 2017;14:2422–36.
[39] Ai X, Sun J, Zhong L, et al. Star-shape redox-responsive PEG-sheddable copolymer of disulfide-linked polyethylene glycol-lysine-di-tocopherol succinate for tumor-triggering intracellular doxorubicin rapid release: head-to-head comparison. Macromol Biosci 2014;14:1415–28.
[40] Yin S, Huai J, Chen X, et al. Intracellular delivery and antitumor effects of a redox-responsive polymeric paclitaxel conjugate based on hyaluronic acid. Acta Biomater 2015;26:274–85.
[41] Qiu LY, Yan L, Zhang L, Jin YM, Zhao QH. Folate-modified poly(2-ethyl-2-oxazoline) as hydrophilic corona in polymeric micelles for enhanced intracellular doxorubicin delivery. Int J Pharm 2013;456:315–24.
[42] Guo H, Zhang D, Li C, et al. Self-assembled nanoparticles based on galactosylated O-carboxymethyl chitosan-graft-stearic acid conjugates for delivery of doxorubicin. Int J Pharm 2013;458:31–8.
[43] Zhang S, Gao H, Bao G. Physical principles of nanoparticle cellular endocytosis. ACS Nano 2015;9:8655–71.
[44] Mao Z, Zhou X, Gao C. Influence of structure and properties of colloidal biomaterials on cellular uptake and cell functions. Biomater Sci 2013;1(9):896–911.
[45] Vercauteren D, Rejman J, Martens TF, Demeester J, De Smedt SC, Braeckmans K. On the cellular processing of non-viral nanomedicines for nucleic acid delivery: mechanisms and methods. J Control Release 2012;161:566–81.
[46] Swanson JA, Watts C. Macropinocytosis. Trends Cell Biol 1995;5:424–8.
[47] Chang J, Jallouli Y, Kroubi M, et al. Characterization of endocytosis of transferrin-coated PLGA nanoparticles by the blood-brain barrier. Int J Pharm 2009;379:285–92.
[48] Zhang J, Sun Y, Tian B, et al. Multifunctional mesoporous silica nanoparticles modified with tumor-shedable hyaluronic acid as carriers for doxorubicin. Colloid Surf B 2016;144:293–302.
[49] Dalla Pozza E, Lerda C, Costanzo C, et al. Targeting gemcitabine containing liposomes to CD44 expressing pancreatic adenocarcinoma cells causes an increase in the antitumoral activity. BBA-Biomembranes 2013;1828:1396–404.
[50] Yang C, Cao M, Liu H, et al. The high and low molecular weight forms of hyaluronan have distinct effects on CD44 clustering. J Biol Chem 2012;287:43094–107.
[51] Zhang G, Zhang H, Liu Y, et al. CD44 clustering is involved in monocyte differentiation. Acta Bioch Bioph Sin 2014;46:540–7.
[52] Wang Y, Yago T, Zhang N, et al. Cytoskeletal regulation of CD44 membrane organization and Interactions with E-selectin. J Biol Chem 2014;289:35159–71.
[53] Perschl A, Lesley J, English N, Trowbridge I, Hyman R. Role of CD44 cytoplasmic domain in hyaluronan binding. Eur J Immunol 1995;25:495–501.
[54] Guo Z, He B, Jin H, et al. Targeting efficiency of RGD-modified nanocarriers with different ligand intervals in response to integrin alphavbeta3 clustering. Biomaterials 2014;35:6106–17.
[55] Culty M, Nguyen HA, Underhill CB. The hyaluronan receptor (CD44) participates in the uptake and degradation of hyaluronan. J Cell Biol 1992;116:1055–62.
[56] Almalik A, Karimi S, Ouasti S, et al. Hyaluronic acid (HA) presentation as a tool to modulate and control the receptor-mediated uptake of HA-coated nanoparticles. Biomaterials 2013;34:5369–80.